Bioprocess Biosyst Eng (2015) 38:917–928
DOI 10.1007/s00449-014-1337-8

ORIGINAL PAPER

Dependence of fungal characteristics on seed morphology and shear stress in bioreactors

Hongzhong Lu · Chao Li · Wenjun Tang · Zejian Wang · Jianye Xia · Siliang Zhang · Yingping Zhuang · Ju Chu · Henk Noorman

Received: 27 October 2014 / Accepted: 7 December 2014 / Published online: 1 January 2015

Abstract The fungal morphology during submerged cultivations has a profound influence on the overall performance of bioreactors. In this research, glucoamylase production by *Aspergillus niger* has been taken as a model to improve more insights. The morphology engineering could be conducted effectively by changing the seed morphology, as well as specific power input. During the fed-batch cultivations, pellet formation under milder shear stress field helped to reduce the broth viscosity, thus relieving oxygen limitation and promoting the enzyme production. Furthermore, we found that the relation between the shear stress field, which was characterized by energy dissipation rate/circulation function (EDCF), and enzyme activity was consistent with quadratic parabola, which threw light on the process optimization and scale-up for industrial enzyme production.

Keywords *Aspergillus niger* · Morphological control · Stirred tank · Mass transfer · Rheology · Hydrodynamics

H. Lu · C. Li · W. Tang · Z. Wang · J. Xia (✉) · S. Zhang · Y. Zhuang · J. Chu (✉)
State Key Laboratory of Bioreactor Engineering, East China University of Science and Technology, P.O. Box 329#, 130 Meilong Road, Shanghai 200237, People's Republic of China
e-mail: jyxia@ecust.edu.cn

J. Chu
e-mail: juchu@ecust.edu.cn

H. Noorman
DSM Biotechnology Center, P.O. Box 1, 2600MA Delft, The Netherlands

List of symbols

C^*	Saturated oxygen concentration in broth (mmol kg^{-1})
CER	Carbon dioxide evolution rate (mmol kg^{-1} h^{-1})
C_L	Oxygen concentration in broth (mmol kg^{-1})
$C_{\varepsilon 1}$, $C_{\varepsilon 1}$, σ_k, σ_ε	Constants in Eqs. (14) and (15)
D	Diameter of impellers (m)
DCW	Dry cell weight (g L^{-1})
DO	Dissolved oxygen tension (–)
EA	Enzyme activity (AGI mL^{-1})
EDCF	Energy dissipation rate/circulation function (W kg^{-1} s^{-1})
$F_{D,lg}$	Interfacial momentum exchange term (kg m s^{-1})
g	Gravity acceleration (m s^{-2})
k_La	Volumetric oxygen mass transfer coefficient (h^{-1})
k_c	Constants in equation
K	Consistency index (Pa s^n)
N	Agitation speed (s^{-1})
n	Flow index (–)
OTR	Gas–liquid mass transfer rate of oxygen (mmol kg^{-1} h^{-1})
OUR	Oxygen uptake rate (mmol kg^{-1} h^{-1})
p	Pressure (Pa)
P_G	Gassed power input (W)
P_{kb}, $P_{\varepsilon b}$	Represent the effects of buoyancy (Pa)
P_{kis}	Turbulence produced by viscous force (Pa)
P_O	Power number (–)
q_{O2}	Specific oxygen uptake rate (mmol g_{DCW}^{-1} h^{-1})
t_c	Circulation time (s)
u_k	Averaged velocity of phase k (m s^{-1})

Greek letters

μ	Specific growth rate (h^{-1})
γ	Shear rate (s^{-1})
ε	Energy dissipation rate ($m^2\ s^{-3}$)
λ_K	Kolmogorov microscale of length (m)
υ_L	Kinematic viscosity of the fluid ($m^2\ s^{-1}$)
μ_{app}	Apparent viscosity ($N\ m^{-2}\ s$)
$\mu_{eff,k}$	Effective viscosity of phase k ($N\ m^{-2}\ s$)
μ_{tl}	Liquid phase turbulence viscosity ($N\ m^{-2}\ s$)
ρ	Density of broth ($kg\ m^{-3}$)
ρ_k	Density of phase k ($kg\ m^{-3}$)
τ	Shear stress ($N\ m^{-2}$)

Introduction

With a GRAS (generally regarded as safe) status, *Aspergillus niger* has been widely employed to produce commercially important products [1–3] such as native or heterologous proteins, organic acids bioactive substances, etc. Being complex and changeable during the process of cultivation, the morphology of *A. niger* comprises mycelia, clumps and pellets [4], which can be engineered by the concentration of spores [5, 6], the shear force [7], the addition of microparticles [8, 9], etc. Usually, the bigger superficial area of mycelia favors the intake of substrates, thus enhancing the cell growth and product formation [10] in comparison with pellets. However, along with the increased biomass, the highly branched network of mycelia could lead to a significant increase in the broth viscosity [11] and even cause a change in properties of cultivation broth [12]. As for industrial glucoamylase production using *A. niger*, the oxygen-limited strategy was preferred to improve the productivity [13]. However, due to the intense oxygen demand, as well as the high broth viscosity, the proper oxygen supply usually became a serious challenge, especially for large-scale fermenters [14].

The fungal morphology is influenced significantly by the hydrodynamic conditions [15]. Generally, the higher specific energy input could enhance the mass transfer [16]. However, if the local shear force induced by higher specific energy input was too intensive, the pellets or clumps could be broken up into mycelia [17, 18] accompanied with the enhancement in broth viscosity, thus counteracting the advantages brought about by raising the specific energy input. A morphological transformation from dispersed mycelia to pellets can also occur during long-time fed-batch cultivations. Studies have shown that depending on the operation conditions, the hyphal elements could increase in size, develop into agglomerates and further into pellets [19]. The broth with pellets is usually accompanied with a lower viscosity and a better fluidity [20]. Currently, computational fluid dynamics (CFD) is highly valuable to depict the flow field within bioreactors under different agitation speed or impeller configurations [21, 22]. With the aid of CFD, the effect of flow field and its distribution on morphological characteristics could be studied comprehensively. Besides, the CFD was also employed to investigate the relationships between fluid dynamics and microbial kinetics [15, 23–25].

In the present work, the effects of seed morphology and specific power input on the pellet size were systematically investigated. Subsequently, the shear stress field in 50-L bioreactors on pelletized morphology and glucoamylase production were further evaluated using two impeller combinations. Finally, the relations between the energy dissipation rate/circulation function (EDCF) and enzyme production were evaluated. The results from this study might throw light on scale-up for viscous fungal fermentations.

Materials and methods

Microorganism and inoculum preparation

Aspergillus niger CBS513.88 producing glucoamylase, was supplied by DSM corporation (Delft, The Netherlands). PDA medium, which contained ($g\ L^{-1}$) glucose·H_2O 2, potato 20, and agar 1.8, was used for the fungi growth. To obtain spores, Petri dishes with PDA medium were incubated with spores from a frozen stock (stored in 50 % glycerin at −80 °C). After 6-day cultivation in a 30 °C incubator, the spore suspension was obtained by rinsing the plates with deionized water. After vortexing, the spore concentration was determined using a counting chamber.

Medium

The medium for seed culture contained ($g\ L^{-1}$) glucose·H_2O 22 and corn steep liquor 20. Before sterilization, the initial pH was adjusted to 6.5 using 3 mol L^{-1} NaOH. A chemically modified medium [13] was used for all cultivations in 50-L fermenter, which contained ($g\ L^{-1}$) glucose·H_2O 45.1, maltodextrin 10, KH_2PO_4 3, $NaH_2PO_4{\cdot}H_2O$ 1.5, $(NH_4)_2SO_4$ 3, $MgSO_4{\cdot}7H_2O$ 1.0, $CaCl_2{\cdot}2H_2O$ 0.1, citric acid 2, $ZnCl_2$ 0.02, $CuSO_4{\cdot}5H_2O$ 0.015, $CoCl_2{\cdot}6H_2O$ 0.015, $MnSO_4{\cdot}H_2O$ 0.04, $FeSO_4{\cdot}7H_2O$ 0.3. After sterilization, the pH was adjusted to 4.5 using 12.5 % NH_4OH. The carbon source in feed medium was composed of glucose monohydrate 163.9 g $L^{-1}$and maltodextrin 50 g L^{-1}, and the remaining composition was the same as the culture medium.

Cultivation

Seed cultivations were carried out in a 15-L stirred tank bioreactor with 8 L of seed medium, inoculated with the spore suspension to a final concentration of 1×10^6 spores per millimeter broth and cultivated for 24 h at 34 °C without pH control. To control the seed in clumps and mycelia, the agitation in the 15-L bioreactor was controlled at 50 and 150 rpm, respectively, and in this case the aeration was adjusted to maintain the same CER (or OUR) level (6 mmol kg^{-1} h^{-1}) at the end of seed cultivations so that the biomass could be kept similar. Subsequently, about 3 L of the seed broth was used to inoculate a 50-L bioreactor. The concentrations of exhaust oxygen and carbon dioxide were measured by a process mass spectrometer (MAX300-LG, Extrel) and the dissolved oxygen in broth was determined by a low-drift polarographic electrode (Mettler Toledo).

Two impeller configures, which were made up of two and three Rushton impellers, respectively, were applied in this work. The diameter of Rushton disk turbine impeller was 0.12 m and the distances between the two adjacent impellers for 2RT and 3RT were 0.24 and 0.12 m, respectively. The impeller power numbers for 2RT and 3RT were 7.7 and 4.6, respectively, which were calculated by [26]:

$$P_O = \frac{P_G}{\rho N^3 D^5}, \tag{1}$$

where P_G is gassed power input (W) measured with a torque meter, ρ is the density of broth, N is the agitation speed and D is the diameter of the impellers.

For all cultivations in 50-L bioreactors, the initial agitation speed was kept at 100 rpm or a smaller value, with pressure maintained at 0.05 MPa and temperature at 34 °C during the whole process. According to DO values, the agitation speed was elevated stepwise until 70 h (except for batches inoculated with clumps) and then remained stable. When the batch culture finished at 44 h, the residual sugar concentration was maintained at 5 g L^{-1} by feeding a sugar solution. The pH was automatically maintained at pH 4.5 by addition of 12.5 % NH_4OH during the cultivation process. All fed-batch cultivations were repeated at least two times.

Enzyme activity assays

Enzyme activity was expressed in amyloglucosidase (AGI) units and was related to an officially assigned amyloglucosidase (glucoamylase) standard. One AGI unit was defined as the amount of enzyme that produced 1 μmol of glucose per minute at pH 4.3 and at 60 °C from a soluble starch substrate. For enzyme activity analysis, 5 mL broth was sampled from the fermenter. After centrifugation, the supernatant was obtained and stored in a 4 °C refrigerator before the measurement. The samples were diluted with acetate dilution buffer (pH 4.3) to a final activity ranging from 8.5 to 42.5 AGI per milliliter. The method for the glucoamylase activity measurement was modified based on [27]. Firstly, 230 μL p-NPG substrate (0.1 g L^{-1}4-nitrophenol-a-D-glucopyranoside (Sigma N-1,377) (pre-warmed for 5 min at 37 °C) was mixed with 20 μL of a diluted culture supernatant sample. After incubation at 37 °C for 20 min, the reaction was quenched by adding 100 μL of 3 mol L^{-1} Na_2CO_3. The absorption of the sample at 405 nm was determined on a micro-plate reader. A control or standard sample was taken along in the experiment to be able to determine the absolute enzyme activity of glucoamylase.

Quantification of biomass

10 mL broth was filtered through pre-dried and preweighted suction filter paper. Before filtering, the filter should be firstly dried to a constant weight (24 h at 80 °C). To remove solutes, the samples were rinsed three times with the deionized water. Then the wet filters with the biomass were put in the 80 °C oven and dried for 24 h. The dried filter was re-weighted immediately.

Quantification of OUR, CER and k_La

Oxygen uptake rate (OUR) and carbon dioxide evolution rate (CER) were determined according a previous report [28]. The specific oxygen uptake rate (q_{O2}) was calculated as follows:

$$q_{O2} = \frac{\text{OUR}}{\text{DCW}}, \tag{2}$$

where DCW is biomass concentration.

The volumetric oxygen mass transfer coefficient (k_La) in bioreactors with oxygen consumption was estimated using the following two formulas [16] using a quasi-steady-state approximation:

$$\frac{dC_L}{dt} = \text{OTR} - \text{OUR} \tag{3}$$

$$\text{OTR} = k_La(C^* - C_L), \tag{4}$$

where C^* is the saturated oxygen concentration in broth, C_L is oxygen concentration in broth and OTR is the gas–liquid mass transfer rate of oxygen.

Quantification of morphological parameters, apparent viscosity, Kolmogorov microscale of length, and the energy dissipation rate/circulation function

The major morphological parameters, including pellets concentration (the number of pellets per milliliter broth), average diameter of pellets, mean total hyphae length and filament ratio were measured using image analysis with Image-Pro Plus 6.0. The detailed description of these morphological parameters can be found in earlier reports [4, 17, 29]. For pelletized morphology analysis, 2 mL of fermentation broth was firstly mixed with 2 mL fixative solution (containing 40 % formaldehyde and 60 % ethanol, v/v) and then stored at 4 °C for the later analysis [30]. To obtain the images of pellets, the mycelia in the sample were discarded. Afterwards, only the pellets were remained, diluted and re-suspended individually in a Petri dish filled with the culture medium. Then the Petri dishes were placed on a desk with a dark background and lit with the neon light. The images of pellets were acquired by the digital camera equipped with a macro-lens. After some pre-treatment, including the enhancement, object recognition and segmentation; the morphological parameters were acquired using the inbuilt analyze particle function in the Image-Pro Plus 6.0. The morphology analysis was automated so that more than 500 pellets could be analyzed for each sample. To calculate the mass ratio of pellets per biomass, the wet pellets were collected on the pre-weighted suction filter paper and dried at 80 °C oven for 24 h.

The impeller spindle (DV-II+, Brookfield Engineering, Stoughton, MA) was used in all rheological tests. The apparent viscosity (μ_{app}) is the shear stress (τ) divided by shear rate (γ), that is

$$\mu_{app} = \frac{\tau}{\gamma}, \tag{5}$$

The equation to calculate the average shear rate in the fermenter was as follows [31]:

$$\gamma = 1.711^{\frac{2.476}{1-n}} \cdot K^{\frac{0.610}{1-n}} \cdot N^{\frac{1.359}{1-n}}, \tag{6}$$

where n is flow index (−), K is consistency index (Pa s^n).

According to the power law model [12]:

$$\tau = K\gamma^n. \tag{7}$$

So,

$$\mu_{app} = K\gamma^{n-1}. \tag{8}$$

To evaluate the effect of shear stress by eddies on the pelletized morphology, the Kolmogorov microscale of length (λ_K) was calculated [32]:

$$\lambda_K = \left(\frac{\upsilon_L^3}{\varepsilon}\right)^{0.25} \tag{9}$$

$$\upsilon_L = \frac{\mu_{app}}{\rho}, \tag{10}$$

where υ_L is the kinematic viscosity of the fluid (m^2 s^{-1}), ε is the specific power input (W kg^{-1}), ρ is fluid density (kg m^{-3}).

To further investigate the shear effects of different impellers, the energy dissipation rate/circulation function (EDCF) was used in this study as the shear force field produced by the impellers is proportional to the energy dissipation rate in the impeller sweeping volume and the frequency of mycelium circulation through that volume [33]. The EDCF was defined as follows [29]:

$$\mathrm{EDCF} = \frac{P_G}{k_c D^3 t_c}, \tag{11}$$

where k_c is geometric constant and t_c is gassed circulation time (s). For the determination of k_c and t_c, we referred to the previously published work [26, 33].

CFD model

The commercial CFD software ANSYS CFX-11 was widely used to simulate the fluid dynamics in a stirred tank reactor [21, 23, 34], and it was also employed in this work. Euler–Euler method was used to simulate two-phase flow, and the continuity equation for each phase can be written as:

$$\frac{\partial}{\partial t}(\rho_k \alpha_k) + \nabla \cdot (\rho_k \alpha_k u_k) = 0, \tag{12}$$

where ρ_k, α_k and $\boldsymbol{u}_k$ are the density, volume fraction and phase averaged velocity, respectively, of the liquid phase (k = l) and gas phase (k = g).

The momentum equation for each phase can be written as:

$$\begin{aligned}&\frac{\partial}{\partial t}(\rho_k \alpha_k u_k) + \nabla \cdot (\rho_k \alpha_k u_k u_k)\\ &= -\alpha_k \nabla p + \nabla \cdot \left[\alpha_k \mu_{\mathrm{eff},k} \times \left(\nabla u_k + \nabla u_k^T\right)\right]\\ &\quad + \rho_k \alpha_k g \pm F_{D,lg},\end{aligned} \tag{13}$$

where g is the gravity acceleration, $F_{D,lg}$ is the interfacial momentum exchange term, $\mu_{\mathrm{eff},k}$ is the effective viscosity of phase k and p is the pressure, shared by both phases.

Other interphase forces like the Bassett force, the virtual mass force and the lift force were neglected in the present study. The interphase drag between gas and liquid and turbulent diffusion force were calculated using the Grace Drag model and the Lopez de Bertodano model, respectively.

As for turbulence modeling, the standard k–ε model was adopted for the continuous phase in the present study. The single phase flow turbulent model can be extended to the multiphase flow turbulent model, therefore, for the continuous phase (liquid):

$$\begin{aligned}\frac{\partial(\alpha_l \rho_l k)}{\partial t} + \nabla \cdot (\alpha_l \rho_l \boldsymbol{u}_l k) = \nabla \cdot \left[\left(\mu + \frac{\mu_{tl}}{\sigma_k}\right)\alpha_l \nabla k\right]\\ + \alpha_l (P_k + P_{kb} - \rho_l \varepsilon)\end{aligned} \tag{14}$$

$$\frac{\partial(\alpha_l \rho_l \varepsilon)}{\partial t} + \nabla \cdot (\alpha_l \rho_l \mathbf{u}_l \varepsilon) = \nabla \cdot \left[\left(\mu + \frac{\mu_{tl}}{\sigma_\varepsilon} \right) \alpha_l \nabla \varepsilon \right] + \alpha_l \frac{\varepsilon}{k} [C_{\varepsilon 1}(P_k + P_{\varepsilon b}) - C_{\varepsilon 2} \rho_l \varepsilon], \tag{15}$$

where $C_{\varepsilon 1}$, $C_{\varepsilon 1}$, σ_k, σ_ε are constants and their values are 1.44, 1.92, 1.0 and 1.3, respectively. μ_{tl} is the liquid phase turbulence viscosity, P_{kb} and $P_{\varepsilon b}$ are used to represent the effects of buoyancy, P_{kis} is the turbulence produced by viscous force.

And for the dispersed phase the "dispersed phase zero equation" model was used, which correlates the turbulence viscosity of the dispersed phase to that of the continuous phase as follows,

$$\mu_{t,g} = \frac{\rho_g}{\rho_l} \frac{\mu_{t,l}}{\sigma}, \tag{16}$$

where σ is the turbulent Prandtl number, of which a default value of 1 was used.

Around 2,000,000 total tetrahedral meshes were used in this model, and the maximum size of each element was about 5 mm. Governing equations were solved using ANSYS CFX-11. The air flow rate was specified as an inlet boundary condition with gas volume fraction of 1 at the location of the air sparger. No-slip boundary conditions were applied on the tank walls and shaft and any other solid surfaces in the flow domain. The free surface of the tank was considered as the degassing boundary condition. The simulations were computed using a cluster with 16 core (Intel Core i5 × 4) cpu and 16 GB DDR memory. Convergence criteria for judging the convergence were a combination of tolerance smaller than 1×10^{-3} and the almost constant whole gas hold-up and axial torque of impeller.

Results and discussion

Effects of seed and specific power input on pelletized morphology

To evaluate the influences of seed morphology, fed-batch cultivations inoculated with clumps and mycelia were firstly conducted. In batches inoculated with clumps, pellet formation occurred since the start of cultivation while in batches inoculated with mycelia, no pellets could be observed before 80 h, indicating that the morphology could be governed effectively by seed morphology. In batches inoculated with clumps, the pellets concentration increased gradually from 600 pellets mL^{-1} at 24 h to 1,055 pellets mL^{-1} at 96 h. However, the average diameter of these pellets was approximately 500 µm since 48 h. It can be seen that, even though with a high DO level, the relatively lower OUR value (Fig. 1b, c) indicated that a fraction of biomass in pelletized morphology was in a low metabolic state. Also, during 0–72 h, the average specific oxygen uptake rate (q_{O2}) for batches of mycelia and clumps was 2.39 and 1.86 mmol/g_{DCW} h, respectively. Due to the fact that the critical transport distance for oxygen penetrating the aggregates was about 200 µm [9], the pellets with the diameter larger than 500 µm in this work certainly resulted in the considerable decrease in the fraction of active biomass. As a result, the enzyme activity and sugar consumption in batches of clumps were reduced by 30 and 15 %, respectively, in contrast with mycelia (Fig. 1d, f).

The negative effects brought by pellet formation indicated that the pellet size should be tailored carefully to reduce the transport limitation within the core of pellets. To control pellet size, a series of cultivations in 5-L fermenters were carried out. The agitations were controlled at 300, 375, 450, 525 and 600 rpm, respectively, while other conditions were fixed. As shown in Fig. 2, there existed a direct correlation between the pellet diameters and P/V (or EDCF), indicating that the pellet size could be determined directly by the specific power input.

Effect of pellet formation on bioreactor performances under oxygen-limited phase

The oxygen-limited strategy was preferred in industrial glucoamylase production. To further investigate the complex interactions among the morphology, shear force and enzyme production under oxygen-limited condition, two impeller combinations, 2RT and 3RT, were employed to investigate the influences of appropriate pellet formation on bioreactor performances. The agitation in 2RT and 3RT was kept at 380 and 360 rpm separately after 72 h and the corresponding specific energy input was 0.96 and 1.34 W kg^{-1}, respectively (Fig. 3). Due to the enhanced agitation speed, the DO was maintained at a relatively high value in first phase from 0 to 72 h, while in the second phase from 72 to 144 h, it was always below the critical value (Fig. 4b). The curves of OUR presented similar tendencies for 2RT and 3RT (Fig. 4a), confirming the good stability and reproducibility under the same inoculum types and process control strategies. During fungal fermentation, the broth viscosity was mainly related to biomass and morphology [35]. As biomass increased, the broth viscosity ascended quickly, reflected by the increased consistent index (K) (Fig. 4f). The negative effects caused by the increased broth viscosity were characterized by the declined OUR levels when specific power input was maintained constant after 60 h (Fig. 3b). Also, due to entanglement of hyphae and accumulation of biomass, the rheology character was changed from the Newtonian liquid to the pseudoplastic as the flow index reduced from 1 at the start of cultivation to 0.3 at the end (Fig. 4e).

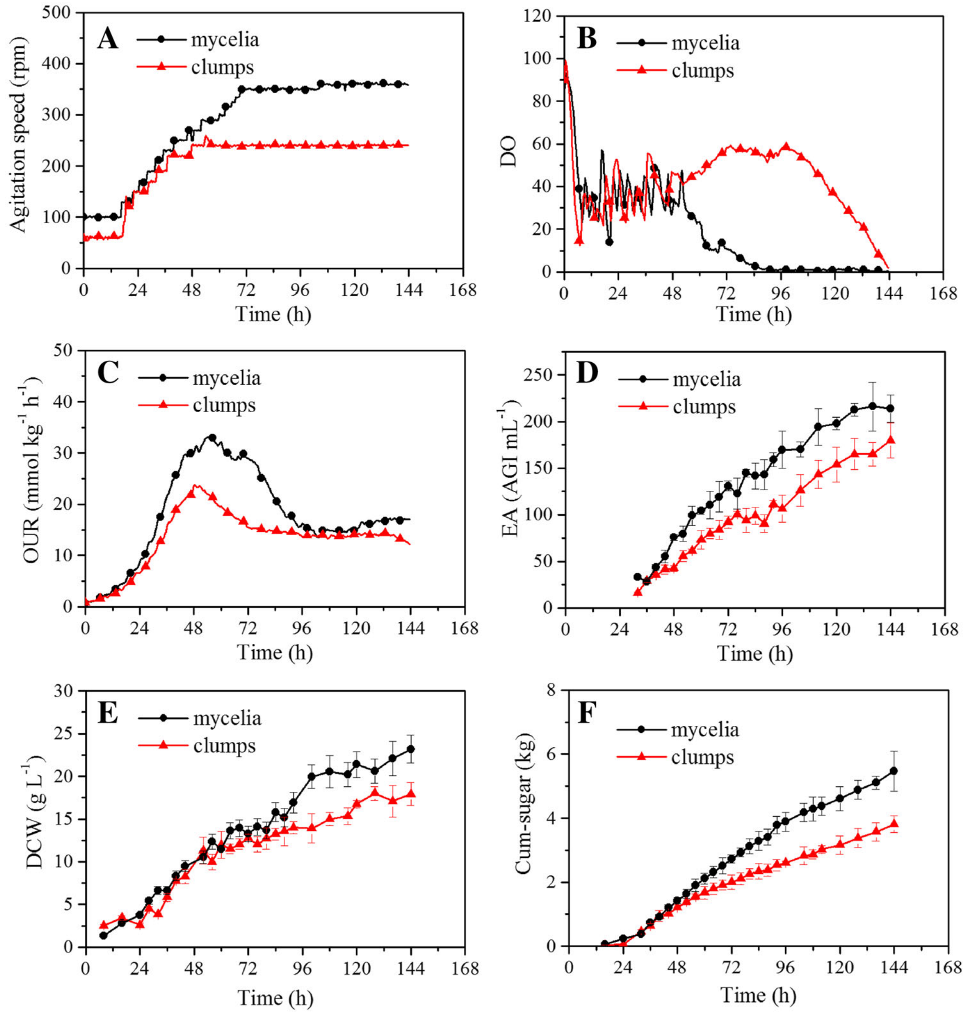

Fig. 1 Profiles of agitation speed (**a**), DO (dissolved oxygen concentration) (**b**), OUR (oxygen uptake rate) (**c**), EA (enzyme activity) (**d**), DCW (dry cell weight) (**e**) and cum-sugar (cumulative consumption of sugar) (**f**) in batches of clumps and mycelia. Clumps (*filled circle*), mycelia (*filled triangle*)

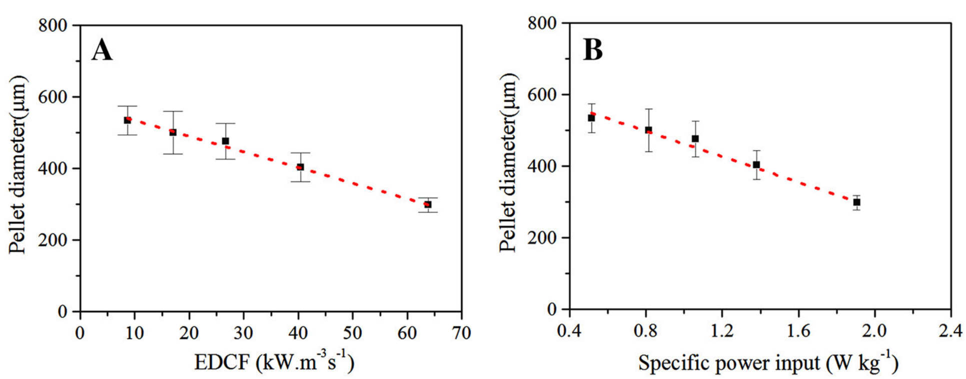

Fig. 2 Pellet diameter in relation to the EDCF (**a**) and specific power input (**b**) in 5-L fermenter

As shown in Fig. 5a, the averaged diameter of pellets in runs of 2RT and 3RT was 410 and 320 μm, respectively, close to the critical diameter of 400 μm [9]. At 120 h, the pellet concentration in batches of 2RT and 3RT, was 640 and 320 pellets mL^{-1}, respectively (Fig. 5b). As the pelletized morphology could slow down the fungal growth [36], the DCW in 2RT was smaller (Fig. 4c). Furthermore, the pelletized morphology favored the significant reduction in broth viscosity compared with mycelia morphology [37–39]. Consequently, the k_La and q_{O2} in batches of 2RT (Fig. 5e, f) were, respectively, 30.7 and 29.2 % higher in comparison with 3RT. The earlier research [37] suggested that the primary effect of morphology on product formation was broth viscosity. As for filamentous fungi, the reduced

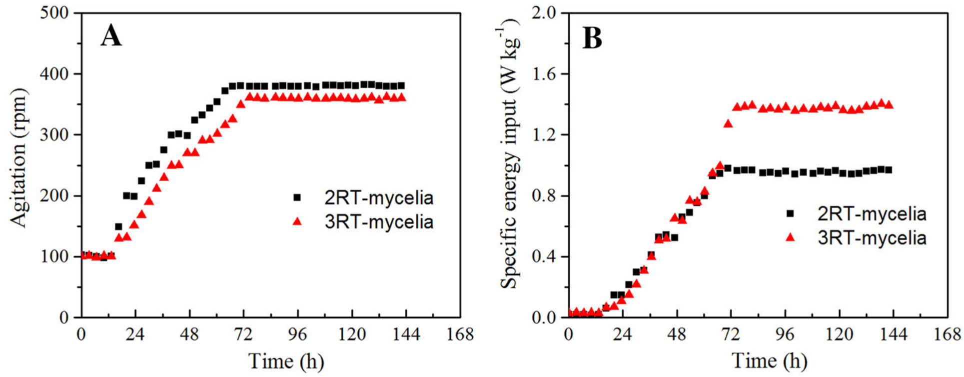

Fig. 3 Profiles of agitation speed (**a**) and specific power input (**b**) in fed-batch fermentations of 3RT and 2RT. 2RT (*filled square*), 3RT (*filled triangle*)

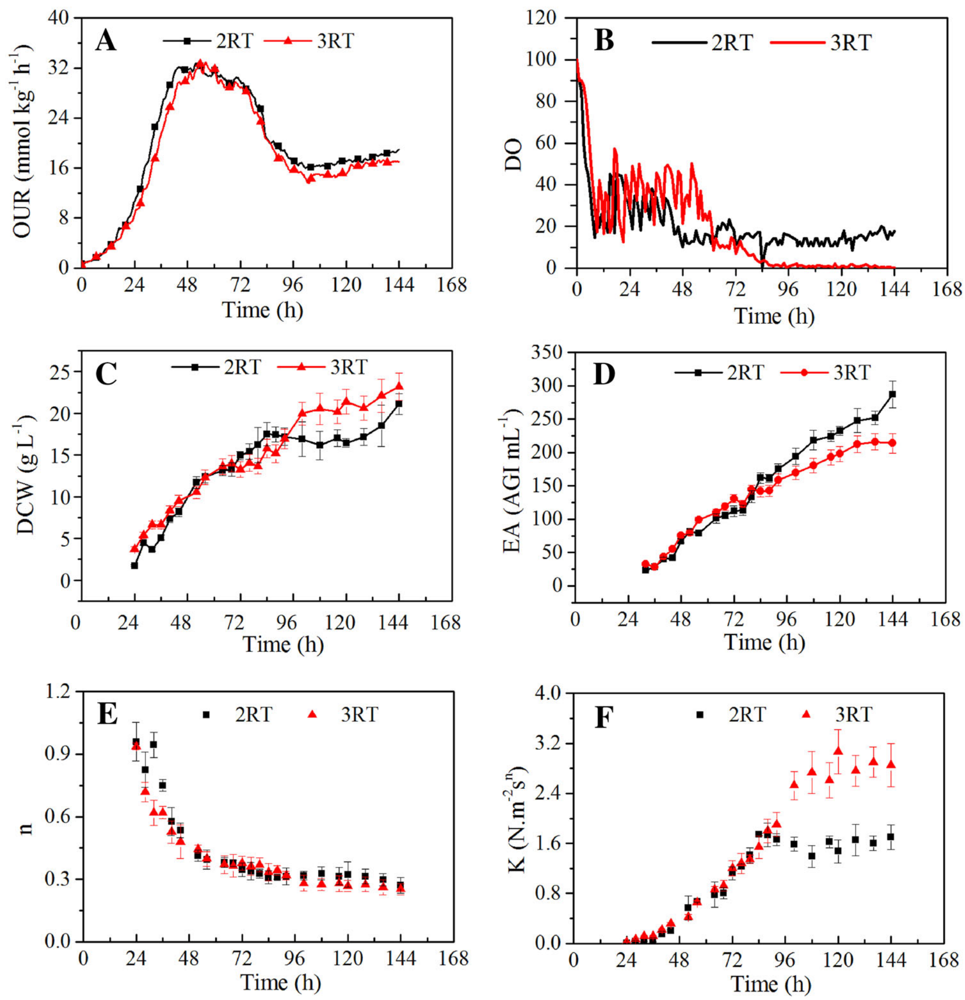

Fig. 4 Profiles of OUR (**a**), DO (**b**), DCW (**c**), EA (**d**), flow index, *n* (**e**) and consistent index, *K* (**f**) in fed-batch fermentations of 3RT and 2RT. 2RT (*filled square*), 3RT (*filled triangle*)

broth viscosity, to some extent, could contribute to the enzyme production [40]. Therefore, the relatively lower broth viscosity brought by the formation of pellets may be responsible for the higher production level in the batches of 2RT.

CFD was often used to depict the holistic distribution of shear stress within larger bioreactors. To clarify the detailed roles played by varied impeller combinations under different specific energy inputs, the fields of liquid velocity and shear strain rate were simulated with CFD. As illustrated in Fig. 6a, the simulated velocity profiles displayed that these two agitator types formed similar flow patterns. Also, the circulation time for 2RT and 3RT was similar, both at about 1.1 s. However, the distribution of

Fig. 5 Comparisons in average diameter of pellet (**a**), pellet concentration (**b**), mass ratio of pellets per biomass (**c**), the average apparent viscosity (**d**), k_La (**e**) and q_{O2} (**f**) for the two impeller combinations of 2RT and 3RT during second phase of cultivation from 80 to 144 h. 2RT (*filled square*), 3RT (*filled triangle*)

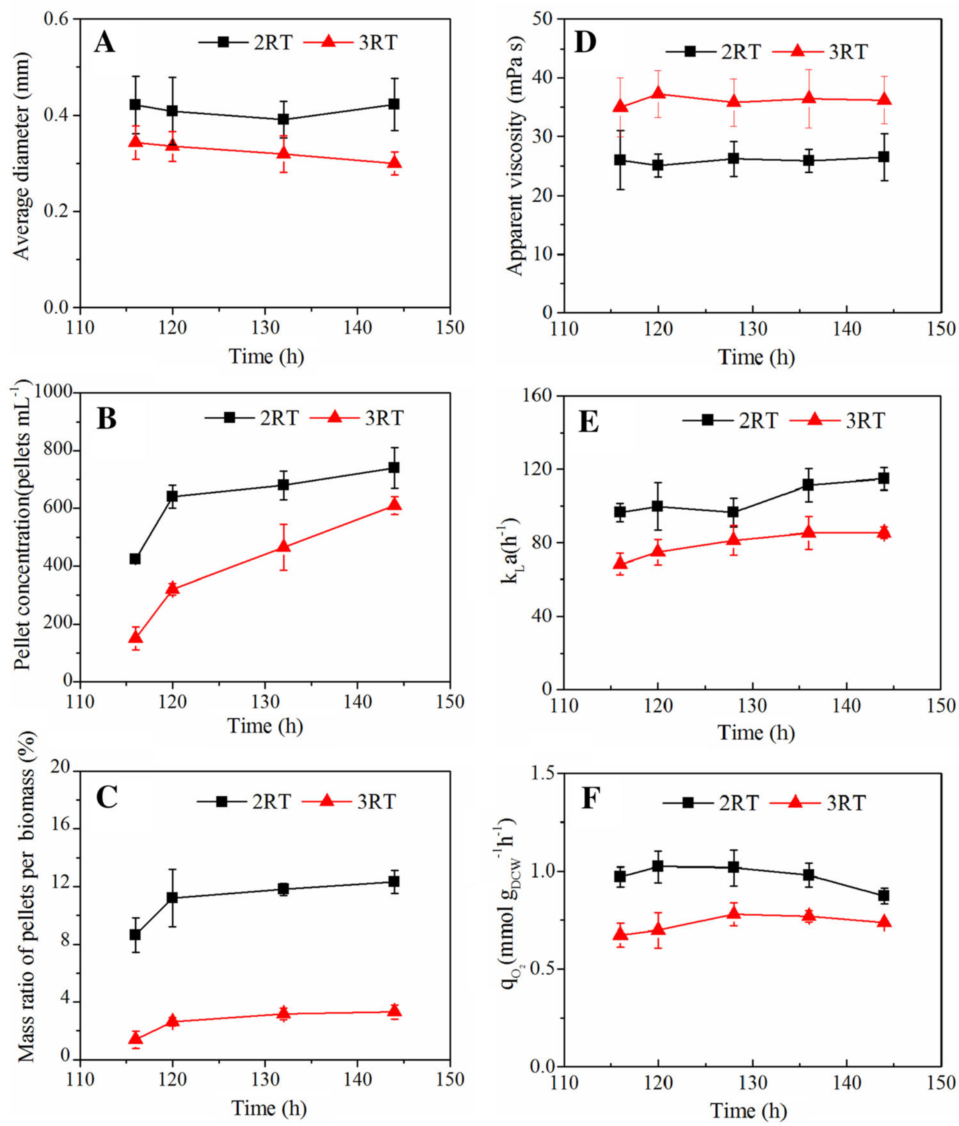

shear strain rate induced by 2RT and 3RT was distinctly different (Fig. 6b). It was observed that the zone of higher shear strain rate within the fermenter equipped with 3RT was larger as each Rushton impeller was accompanied with a zone of high shear rate. Overall, the simulated energy dissipation rate (ε) of 2RT and 3RT was 0.29 and 0.43 $m^2\ s^{-3}$, respectively, indicating that the shear stress induced by 3RT was stronger. As the smallest eddies determine the size of pellets in stirred tank reactors [32], the Kolmogorov microscale of length (λ_K) was calculated. The λ_K in fermenters equipped with 2RT and 3RT were 900 and 870 µm, respectively, which was in the same magnitude of pellet size in this study, thus it could be concluded that the pellet size was mainly affected by the fluid induced shear stress by eddies within fermenters. Generally, the too intensive shear stress could lead to the reduction in growth [41], thus, in turn, bringing adverse effects. However, in this study, the shear force induced by 3RT was not strong enough to inhibit the growth of *A. niger* due to the fact that the biomass concentration in batches of 3RT was higher than 2RT during late phase of cultivation (Fig. 4c). So combining the CFD simulation with the morphological analysis, it could be concluded that the milder shear stress environment of 2RT favored the pellet formation, which in turn resulted in better enzyme production.

EDCF as a guide for fungi scale-up

Generally, the synthetic effects of local shear stress and mixing time within the fermenters on cell physiology could be characterized by energy dissipation rate/circulation

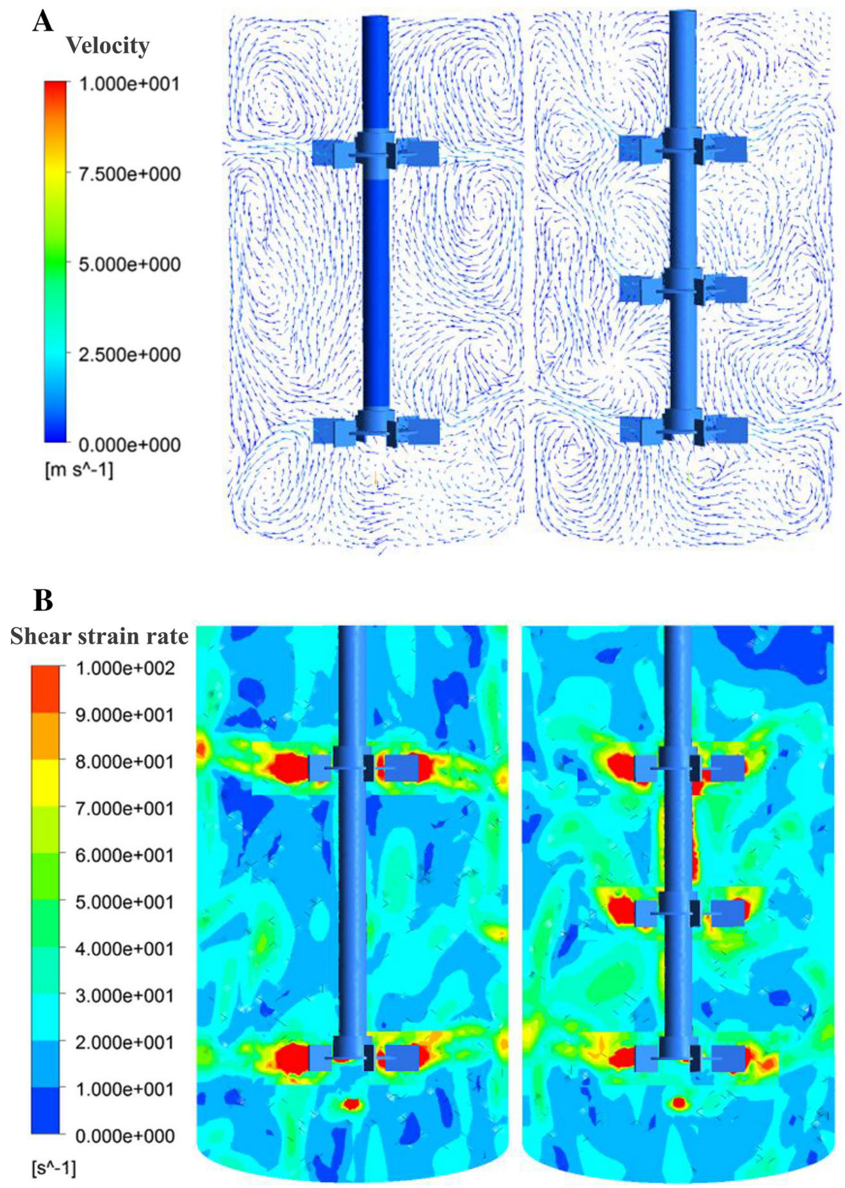

Fig. 6 Flow field of velocity (**a**) and shear strain rate (**b**) from CFD simulations for the impeller combinations of 2RT and 3RT. The color of *red* and *dark blue* denotes highest value and the lowest, respectively. The impeller rotation speed in CFD was equal to the value used in the actual cultivation that is 380 rpm for 2RT and 360 rpm for 3RT. The CFD simulations were conducted under the similar rheological parameters before 80 h (color figure online)

function (EDCF). In large-scale fermenters, the EDCF values were quite different at different positions or with different impeller combinations [23, 26]. For the fungal fermentation, the cell physiology could vary greatly under different local EDCF values [42, 43], thus it is very important to evaluate the effect of EDCF on morphology and enzyme production in small-scale fermenters, which could provide useful clues for process optimization and scale-up. As reported by Jüsten [33], the correlation between the morphological parameters and EDCF could be established under different scales of fermenters using the cold model experiments. However, the influences of EDCF on production under real fed-batch cultivations were vague. To describe the relations between the shear stress environment and enzyme production, the cultivations under different impeller configurations and scales in our lab were summarized (Table 1).

As described in Fig. 7b, the effects of tip speed on enzyme production were inconspicuous, which may be due to the differences in impeller configurations and bioreactor scales. It should be noted that a direct relation between the enzyme activity and shear rate (or specific power input) existed but some overlapping data points existed (Fig. 7a, c). By comparison, the relation between the EDCF and enzyme activity was more relevant as it was consistent with the quadratic parabola. The reason for the increased enzyme activity (Fig. 7d) may be explained by the higher k_La under larger EDCF values [29]. On the contrary, the decreased enzyme activity may be due to the pellet breakup [17] or growth inhibition [41] caused by the strong shear

Table 1 Summary of fed-batch cultivations in 50-L and 5-L fermenters

Cultivations	P/V (W/kg)	EDCF (kW $m^{-3}s^{-1}$)	Tip speed (m s^{-1})	Shear rate (s^{-1})	Enzyme activity[a] (AGI mL^{-1})
50L-2RT-360rpm	0.82	20.00	2.26	374.04	255 ± 20
50L-3RT-380rpm	1.62	28.00	2.39	458.40	197 ± 10
50L-3RT-335rpm	1.10	17.00	2.10	439.719	256 ± 24
50L-3RT-240rpm	0.27	5.06	1.51	165.69	154 ± 10
50L-3Whu[b]-470rpm	0.84	14.00	2.07	642.11	230 ± 13
50L-HBT[c]+2Whu-330rpm	0.54	9.33	2.07	384.76	214 ± 28
5L-2RT-300rpm	0.52	8.66	1.10	249.82	165 ± 13
5L-2RT-375rpm	0.82	17.09	1.37	494.35	263 ± 21
5L-2RT-450rpm	1.06	26.66	1.65	702.79	209 ± 14

[a] The enzyme activity was measured at 120 h

[b] *Whu* three wide-blade hydrofoil impeller pumping up

[c] *HBT* hollow blade turbine

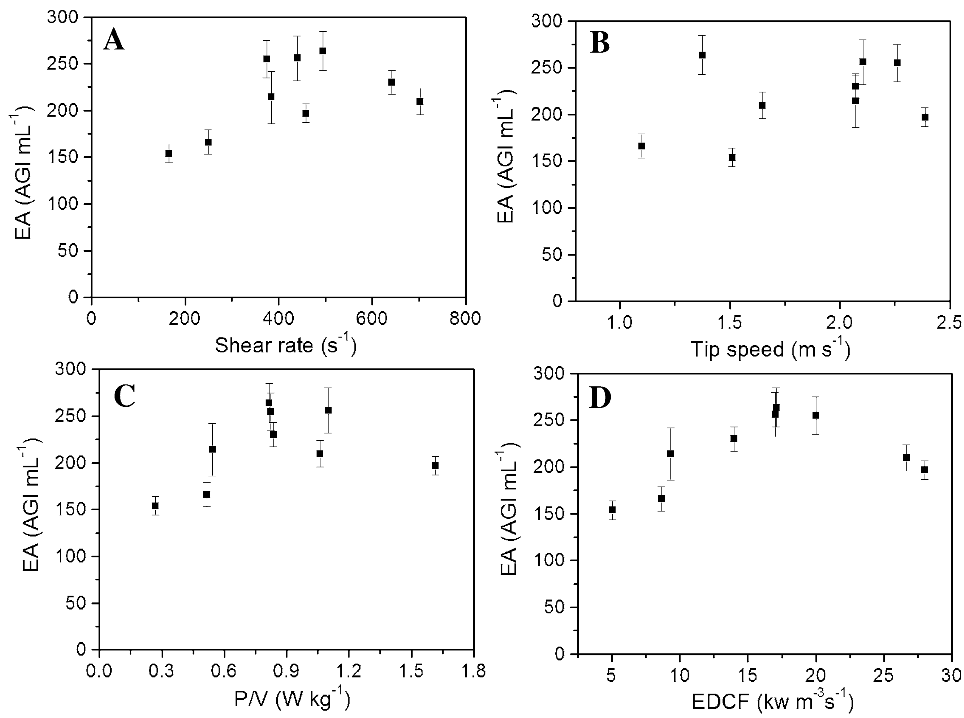

Fig. 7 Enzyme activity in relation to the shear rate (**a**), tip speed (**b**), specific power input (**c**) and EDCF (**d**)

force. So we think, under oxygen-limited condition, the effect of EDCF on performances of bioreactors was much more remarkable than other parameters. Hence, the effect of the shear stress environment characterized by EDCF on the enzyme production was firstly illustrated during fed-batch cultivations.

Conclusion

The efficiency of glucoamylase production was closely related to the control of morphology as both the mass transfer and microbial growth were affected significantly by morphological parameters. By integrating the seed morphology and specific power input, the morphology engineering could be carried out to reduce the pellet size, thus reducing the oxygen limitation within the core of pellets. The milder shear stress field could facilitate proper pellets formation, which could help to relieve the limitation in oxygen supply in the late phase of fermentation. To describe the effects of process parameters on the final production level, the relation between the enzyme production and EDCF/tip speed/average shear rate/specific power input was analyzed, respectively. We found that the optimum EDCF existed; hence, it could be scale-up criteria for fungal fermentation. Further work should be conducted to combine the fluid hydrodynamic with the growth kinetic of *A. niger* to improve the performances of large-scale fermenters.

Acknowledgments This work was financially supported by Royal DSM (Delft, the Netherlands) and partially supported by NWO-MoST Joint Program (2013DFG32630), National Basic Research Program (973 Program 2013CB733600), National High Technology Research and Development Program of China (863 Program 2012AA021201) and National Key Technology R&D Program (2012BAI44G01). We would like to thank Sybe Hartmans, Qing Yuan Yin and Jie Zhao for their kind concern on this project.

References

1. Meyer V, Wu B, Ram AFJ (2011) *Aspergillus* as a multi-purpose cell factory: current status and perspectives. Biotechnol Lett 33:469–476
2. Lubertozzi D, Keasling JD (2009) Developing *Aspergillus* as a host for heterologous expression. Biotechnol Adv 27:53–75
3. Ganzlin M, Rinas U (2008) In-depth analysis of the *Aspergillus niger* glucoamylase (*gla*A) promoter performance using high-throughput screening and controlled bioreactor cultivation techniques. J Biotechnol 135:266–271
4. Paul GC, Thomas CR (1998) Characterisation of mycelial morphology using image analysis. In: Schügerl K (ed) Relation Between Morphology and Process Performances. Springer, Berlin Heidelberg
5. Papagianni M, Mattey M (2006) Morphological development of *Aspergillus niger* in submerged citric acid fermentation as a function of the spore inoculum level. Application of neural network and cluster analysis for characterization of mycelial morphology. Microb Cell Fact 5:3–15
6. Liao W, Liu Y, Frear C, Chen S (2007) A new approach of pellet formation of a filamentous fungus - *Rhizopus oryzae*. Bioresour Technol 98:3415–3423
7. Kelly S, Grimm LH, Hengstler J, Schultheis E, Krull R, Hempel DC (2004) Agitation effects on submerged growth and product formation of *Aspergillus niger*. Bioprocess Biosystems Eng 26:315–323
8. Driouch H, Hänsch R, Wucherpfennig T, Krull R, Wittmann C (2012) Improved enzyme production by bio-pellets of *Aspergillus niger*: targeted morphology engineering using titanate microparticles. Biotechnol Bioeng 109:462–471
9. Driouch H, Sommer B, Wittmann C (2010) Morphology Engineering of *Aspergillus niger* for Improved Enzyme Production. Biotechnol Bioeng 105:1058–1068
10. Oncu S, Tari C, Unluturk S (2007) Effect of Various Process Parameters on Morphology, Rheology, and Polygalacturonase Production by *Aspergillus sojae* in a Batch Bioreactor. Biotechnol Prog 23:836–845
11. Riley GL, Tucker KG, Paul GC, Thomas CR (2000) Effect of biomass concentration and mycelial morphology on fermentation broth rheology. Biotechnol Bioeng 68:160–172
12. Wucherpfennig T, Kiep KA, Driouch H, Wittmann C, Krull R (2010) Morphology and Rheology in Filamentous Cultivations. Adv Appl Microbiol 72:89–136
13. Pedersen L, Hansen K, Nielsen J, Lantz AE, Thykaer J (2011) Industrial glucoamylase fed-batch benefits from oxygen limitation and high osmolarity. Biotechnol Bioeng 109:116–124
14. Garcia-Ochoa F, Gomez E (2009) Bioreactor scale-up and oxygen transfer rate in microbial processes: an overview. Biotechnol Adv 27:153–176
15. Yu L, Chao Y, Wensel P, Chen S (2012) Hydrodynamic and kinetic study of cellulase production by *Trichoderma reesei* with pellet morphology. Biotechnol Bioeng 109:1755–1768
16. Gabelle JC, Jourdier E, Licht RB, Ben Chaabane F, Henaut I, Morchain J, Augier F (2012) Impact of rheology on the mass transfer coefficient during the growth phase of *Trichoderma reesei* in stirred bioreactors. Chem Eng Sci 75:408–417
17. Cui YQ, van der Lans RGJM, Luyben KCAM (1997) Effect of agitation intensities on fungal morphology of submerged fermentation. Biotechnol Bioeng 55:715–726
18. Marten MR, Li ZJ, Shukla V, Fordyce AP, Pedersen AG, Wenger KS (2000) Fungal morphology and fragmentation behavior in a fed-batch *Aspergillus oryzae* fermentation at the production scale. Biotechnol Bioeng 70:300–312
19. Nielsen J, Johansen CL, Jacobsen M, Krabben P, Villadsen J (1995) Pellet formation and fragmentation in submerged cultures of *Penicillium chrysogenum* and its relation to penicillin production. Biotechnol Prog 11:93–98
20. Krull R, Wucherpfennig T, Esfandabadi ME, Walisko R, Melzer G, Hempel DC, Kampen I, Kwade A, Wittmann C (2013) Characterization and control of fungal morphology for improved production performance in biotechnology. J Biotechnol 163:112–123
21. Li X, Zhang J, Tan YL, Li ZH, Yu XF, Xia JY, Chu J, Ge YQ (2013) Effects of flow field on the metabolic characteristics of *Streptomyces lincolnensis* in the industrial fermentation of lincomycin. J Biosci Bioeng 115:27–31
22. Yang YM, Xia JY, Li JH, Chu J, Li L, Wang YH, Zhuang YP, Zhang SL (2012) A novel impeller configuration to improve fungal physiology performance and energy conservation for cephalosporin C production. J Biotechnol 161:250–256
23. Xia JY, Wang YH, Zhang SL, Chen N, Yin P, Zhuang YP, Chu J (2009) Fluid dynamics investigation of variant impeller combinations by simulation and fermentation experiment. Biochem Eng J 43:252–260
24. Vrábel P, van der Lans RGJM, van der Schot FN, Luyben KCAM, Xu B, Enfors S-O (2001) CMA: integration of fluid dynamics and microbial kinetics in modelling of large-scale fermentations. Chem Eng J 84:463–474
25. Moilanen P, Laakkonen M, Aittamaa J (2006) Modeling Aerated Fermenters with Computational Fluid Dynamics. Ind Eng Chem Res 45:8656–8663
26. Jüsten P, Paul GC, Nienow AW, Thomas CR (1998) Dependence of *Penicillium chrysogenum* growth, morphology, vacuolation, and productivity in fed-batch fermentations on impeller type and agitation intensity. Biotechnol Bioeng 59:762–775
27. Nielsen J, Pedersen H, Beyer M (2000) Glucoamylase production in batch, chemostat and fed-batch cultivations by an industrial strain of *Aspergillus niger*. Appl Microbiol Biotechnol 53:272–277
28. Wang ZJ, Wang HY, Li YL, Chu J, Huang MZ, Zhuang YP, Zhang SL (2010) Improved vitamin B12 production by step-wise reduction of oxygen uptake rate under dissolved oxygen limiting level during fermentation process. Bioresour Technol 101:2845–2852
29. Casas López JL, Sánchez Pérez JA, Fernández Sevilla JM, Rodríguez Porcel EM, Chisti Y (2005) Pellet morphology, culture rheology and lovastatin production in cultures of *Aspergillus terreus*. J Biotechnol 116:61–77
30. Papagianni M, Mattey M, Kristiansen B (1999) The influence of glucose concentration on citric acid production and morphology of *Aspergillus niger* in batch and culture. Enzyme Microb Technol 25:710–717
31. Campesi A, Cerri M, Hokka C, Badino A (2009) Determination of the average shear rate in a stirred and aerated tank bioreactor. Bioprocess Biosystems Eng 32:241–248
32. Kelly S, Grimm LH, Bendig C, Hempel DC, Krull R (2006) Effects of fluid dynamic induced shear stress on fungal growth and morphology. Process Biochem 41:2113–2117
33. Jüsten P, Paul GC, Nienow AW, Thomas CR (1996) Dependence of mycelial morphology on impeller type and agitation intensity. Biotechnol Bioeng 52:672–684

34. Ranganathan P, Sivaraman S (2011) Investigations on hydrodynamics and mass transfer in gas–liquid stirred reactor using computational fluid dynamics. Chem Eng Sci 66:3108–3124
35. Wucherpfennig T, Kiep KA, Driouch H, Wittmann C, Krull R (2010) Morphology and rheology in filamentous cultivations. In: Allen I. Laskin SS, Geoffrey MG (eds) Advances in Applied Microbiology. Academic Press
36. Paul GC, Priede MA, Thomas CR (1999) Relationship between morphology and citric acid production in submerged *Aspergillus niger* fermentations. Biochem Eng J 3:121–129
37. Johansen CL, Coolen L, Hunik JH (1998) Influence of Morphology on Product Formation in *Aspergillus awamori* during Submerged Fermentations. Biotechnol Prog 14:233–240
38. Galaction AI, Cascaval D, Oniscu C, Turnea M (2004) Prediction of oxygen mass transfer coefficients in stirred bioreactors for bacteria, yeasts and fungus broths. Biochem Eng J 20:85–94
39. Porcel EMR, Lopez JLC, Perez JAS, Sevilla JMF, Chisti Y (2005) Effects of pellet morphology on broth rheology in fermentations of *Aspergillus terreus*. Biochem Eng J 26:139–144
40. Marten MR, Bhargava S, Nandakumar MP, Roy A, Wenger KS (2003) Pulsed feeding during fed-batch fungal fermentation leads to reduced viscosity without detrimentally affecting protein expression. Biotechnol Bioeng 81:341–347
41. El-Enshasy H, Kleine J, Rinas U (2006) Agitation effects on morphology and protein productive fractions of filamentous and pelleted growth forms of recombinant *Aspergillus niger*. Process Biochem 41:2103–2112
42. Rocha-Valadez JA, Galindo E, Serrano-Carreón L (2007) The influence of circulation frequency on fungal morphology: a case study considering Kolmogorov microscale in constant specific energy dissipation rate cultures of *Trichoderma harzianum*. J Biotechnol 130:394–401
43. Li ZJ, Shukla V, Wenger KS, Fordyce AP, Pedersen AG, Marten MR (2002) Effects of increased impeller power in a production-scale *Aspergillus oryzae* fermentation. Biotechnol Prog 18:437–444